Eur. Phys. J. D **8**, 117–124 (2000)

THE EUROPEAN PHYSICAL JOURNAL D

EDP Sciences

Spatial and temporal properties of parametric fluorescence around degeneracy in a type I LBO crystal

F. Devaux[a] and E. Lantz

Laboratoire d'Optique P.M. Duffieux, Centre National de la Recherche Scientifique[b], Université de Franche-Comté, 25030 Besançon Cedex, France

Received 18 February 1999 and Received in final form 9 June 1999

Abstract. We present a theoretical and experimental study of the spatio-temporal properties of the spontaneous parametric emission generated in a type I LBO crystal around degeneracy. The number of quasi-phase-matched modes is shown to be equal to the number of spatio-temporal degrees of freedom of the image that can be parametrically amplified. From this number, we demonstrate the possibility of predicting the total number of photons generated by parametric fluorescence. Correlation is observed between spatial intensity fluctuations corresponding to pairs of signal-idler modes.

PACS. 42.65.Yj Optical parametric oscillators and amplifiers – 42.50.Lc Quantum fluctuations, quantum noise and quantum jumps

1 Introduction

Optical parametric fluorescence was theoretically predicted in 1961 by Louisell [1] and experimentally observed a few years later [2–4]. In 1968, Byer and Harris [5] calculated the power of spontaneous parametric emission by assuming a collimated pump plane wave interacting in the $\chi^{(2)}$ crystal with one photon per each black body mode. Only modes corresponding to a phase matched interaction actually radiate. This model was used for the measurements of nonlinear coefficients of crystals [5] and quasi-phase-matched (QPM) waveguides [6]. These measurements involved the detection of fluorescence within a limited acceptance angle around the colinear propagation with the pump beam and integration over a wide wavelength bandwidth [7] assuming no degeneracy between the signal and idler wavelengths. An alternative measurement scheme was reported in 1994 by Koch *et al.* [8,9], where a monochromator is used to detect the fluorescence cone of non colinear phase matching at a precise wavelength. No degeneracy between the signal and the idler was also assumed. Weighting the fluorescence modes by their phase matching efficiency corresponds to studying phase matching in parametric image amplification, where the spatial resolution is determined by the angular acceptance of the signal, with a collimated pump [10]. In the second part of the paper, we will actually show that the notion of phase matched spatial mode is exactly equivalent to that of resolution cell in image amplification. This conclusion can be extended in the temporal domain, leading to a complete equivalence between the notion of quantum mode and that of spatio-temporal resolution cell in an optical amplifier. As shown by Prasad [11], this equivalence precludes efficient optical amplification of incoherent (thermal) light.

The third part of the paper is devoted to the theoretical and numerical study of the parametric fluorescence in a LBO crystal ($LiBO_5$: *triborate lithium*) near degeneracy. This regime was excluded in the previous studies [5,8,12].

Experimental results concerning the fluorescence mean power are presented in the fourth part of the paper. Last, an analysis of the spatial fluctuations is presented in the fifth part.

2 Quantum modes and spatio-temporal degrees of freedom of monochromatic light

We have shown [13] previously that parametric amplification of a monochromatic image acts on an image either as a low, or a band pass filter, depending on the orientation of the crystal. In a low-pass configuration, *i.e.* around perfect colinear phase matching, the amplification efficiency remains greater than 44% [14] in a solid angle $\Delta\Omega = \pi\Delta\Phi^2$ with $\Delta\Phi$ the maximum internal angle of the signal. By the laws of Fourier Optics, $\Delta\Phi$ can be associated with a resolution cell on the transverse section of the crystal whose radius is given by:

$$R = \frac{0.31\lambda}{n \sin \Delta\Phi}, \tag{1}$$

where n is the refractive index of the crystal and λ the vacuum wavelength. Hence, the number of resolved points

[a] e-mail: fabrice.devaux@univ-fcomte.fr
[b] Unité Mixte de Recherche 6603

in the paraxial approximation is given by:

$$N = \frac{S}{\pi R^2} = \frac{Sn^2 \Delta\Omega}{0.31^2 \pi^2 \lambda^2}, \tag{2}$$

where S is the cross-section of the interaction volume within the crystal. For a signal of duration Δt, with a frequency bandwidth $\Delta\nu$ sufficiently narrow to allow the phase matching condition not to be modified, the total number of spatio-temporal degrees of freedom is:

$$N_{\text{total}} = N \Delta t \Delta\nu = \frac{n^2 S \Delta t \Delta\nu \Delta\Omega}{0.31^2 \pi^2 \lambda^2}\,. \tag{3}$$

Clearly equation (3) remains valid for a band-pass configuration, where $\Delta\Omega$ is a ring centered on the direction of the pump wavevector in a type I configuration. On the other hand, the number of signal modes associated with directions inside the solid angle $\Delta\Omega$ which leave the crystal during Δt is:

$$N_{\Delta t} = N_m \frac{c \Delta t \Delta\Omega}{4\pi n L}, \tag{4}$$

where L is the length of the interaction volume V and N_m is the number of modes in this volume in a frequency range $[\nu;\, \nu + \mathrm{d}\nu]$:

$$N_m = \frac{4\pi V k^2 \mathrm{d}k}{(2\pi)^3}, \tag{5}$$

with $k = 2\pi n/\lambda$. Equations (3, 4) give the same result.

To conclude this section, the number of quantum modes that experience QPM amplification is also the number of spatio-temporal degrees of freedom of the image that can be amplified.

3 Theoretical estimation of the parametric fluorescence power

In a parametric interaction, only photons generated in QPM modes lead to amplification. The total mean number of photons generated at the output of the crystal is equal to:

$$\overline{n}_{\text{ph}} = \Delta t S c \iint \frac{n^2 G(\Phi, \Theta, \lambda)}{\lambda^4} \mathrm{d}\lambda\, \mathrm{d}\Omega, \tag{6}$$

where Δt is the time duration of the fluorescence signal, $G(\Phi,\, \Theta,\, \lambda)$ is the gain for a mode of the vacuum, with one photon per mode at the input. The angles $(\Phi,\, \Theta)$ describe the direction of propagation with respect to the crystal axes of the wavevector $\mathbf{k}_m$ associated to a spatio-temporal mode m. Quantum mechanical treatment of the optical parametric interaction gives, in the undepleted pump approximation with no input signal, the mean number of photons at the output of the nonlinear crystal for the mode m [15]:

$$G(\Phi_m,\, \Theta_m,\, \lambda_m) = (\gamma \Gamma)^2, \tag{7}$$

where

$$\gamma = \frac{g}{K} \begin{cases} g > \dfrac{\Delta k}{2},\ K = \sqrt{g^2 - \left(\dfrac{\Delta k}{2}\right)^2}, \\ \qquad\qquad \Gamma = \sinh(KL), \\ g \le \dfrac{\Delta k}{2},\ K = \sqrt{\left(\dfrac{\Delta k}{2}\right)^2 - g^2}, \\ \qquad\qquad \Gamma = \sin(KL). \end{cases} \tag{8}$$

The phase mismatch Δk is given by:

$$\Delta k = |\Delta \mathbf{k}| = |\mathbf{k}_p - \mathbf{k}_m - \mathbf{k}_{m'}|, \tag{9}$$

where $\mathbf{k}_p$ is the wavevector associated with the single-mode pump and $\mathbf{k}_{m'}$ is the wavevector associated with the spatio-temporal "idler" mode m' of the vacuum which minimizes the phase mismatch. The parametric gain g is equal to:

$$g = \left(\frac{2\, \omega_m\, \omega_{m'}\, d_{\text{eff}}^2\, I_{\text{pump}}}{n_m\, n_{m'}\, n_{\text{pump}}\, \varepsilon_0\, c^3} \right)^{\frac{1}{2}}, \tag{10}$$

where d_{eff} is the effective nonlinear coefficient, $(\omega_\alpha,\, n_\alpha)$ are respectively the frequency and the refractive index of a mode α. I_{pump} is the pump intensity which is assumed to be constant during the time duration of the fluorescence signal. In a birefringent crystal, the modulus of the wavevector depends on the effective refractive index seen by the light. Therefore, it depends on the polarization of the electric field and on the direction of propagation of the wavevector. In our experiments, with a type I LBO crystal, the parametric fluorescence signal is perpendicularly polarized to the (XY) plane of the crystal. Hence, we assume that the effective refractive index seen by the fluorescence remains constant ($n_m = n_{m'} = n_z(\lambda_m)$) whatever the direction of propagation $(\Phi_m,\, \Theta_m)$ around complete degeneracy ($\lambda_m = 2\lambda_{\text{p}}$, $\Phi_m = \Phi_{\text{p}}$, and $\Theta_m = \Theta_{\text{p}} = 90°$). From the gain $G(\Phi,\, \Theta,\, \lambda)$ we define the amplification transfer function (ATF) for spatio-temporal modes [13,16], by the ratio:

$$ATF(\Phi,\, \Theta,\, \lambda) = \frac{G(\Phi,\, \Theta,\, \lambda)}{G_0}, \tag{11}$$

where G_0 is the gain for a perfect phase matched mode at degeneracy.

Figures 1a and 1b show, in gray levels, the amplification transfer function $ATF_{\lambda_0}(\Phi,\, \Theta)$ calculated at degeneracy ($\lambda_m = 2\lambda_{\text{p}} = 1064$ nm) for two different propagation directions of the pump plane wave in the (XY) LBO crystal plane ($\Theta_{\text{p}} = 90°$). The crystal is 15 mm long, $d_{\text{eff}} = 0.96\ \text{pm V}^{-1}$ and the mean parametric gain is equal to 10 cm^{-1}. For Φ_{p} lower than 11° no light is generated at 1064 nm. When Φ_{p} increases, the fluorescence signal is first emitted in a cone (Fig. 1a) and then in a ring (Fig. 1b) always centered on the pump wave direction. The size of a spatial mode depends on the characteristics of the pump pulse and we will calculate its exact dimensions in the experimental part of the paper. In this part we assume

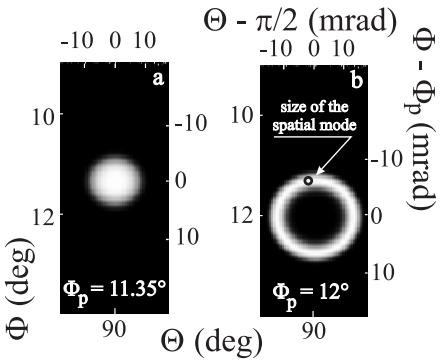

Fig. 1. Results showing in gray levels the amplification transfer function calculated at degeneracy ($\lambda_0 = 2\lambda_\mathrm{p} = 1064$ nm) for different angles Φ_p of the pump direction in the (XY) LBO crystal plane. The elementary cell representing a spatial fluorescent mode is shown in (b).

Table 1. Number of quasi-phase matched spatial modes calculated for different phase matching conditions.

Φ_p (°)	11.1	11.2	11.35	11.5	11.7	11.9	12.3
N_spatial	0	15	51	88	101	103	101

that the radius of the spatial mode is equal to 1 mrad. We have drawn in Figure 1b the corresponding elementary cell. The number of QPM modes N_spatial is obtained for a given phase matching condition by dividing the QPM area by the size of a mode:

$$N_\mathrm{spatial} = \frac{\text{QPM area}}{\text{spatial mode size}} \cdot \tag{12}$$

As indicated in Section 2, the QPM area is the surface of the ATF where efficiency remains greater than 44% (for a parametric gain of 10 cm^{-1} it corresponds to a phase mismatch $\Delta k_0 \simeq 5$ cm^{-1}). The number of QPM spatial modes has been calculated for different phase matching conditions (Tab. 1). This number evolves from 0, when the pump angle Φ_p does not permit phase matching, to a constant approximately equal to 100. Around colinear phase matching ($\Phi_\mathrm{p} = 11.35°$), its value is 50, *i.e.* half the maximum value. Such results can be analytically demonstrated. Indeed, the parametric fluorescence always sees the same refractive index whatever its direction and its divergence $\Delta\Phi_0$ around the degenerated colinear phase-matching configuration obeys the condition (see Fig. 2a):

$$\Delta k_0 = |\mathbf{k}_\mathrm{p} - \mathbf{k}_m - \mathbf{k}_{m'}| \simeq |k_\mathrm{p}|(1 - \cos\Delta\Phi_0), \tag{13}$$

where $\Delta\Phi_0$ is a small angle. The solid angle where fluorescence attains 44% of its maximum value is given by:

$$\Delta\Omega_0^\mathrm{c} = \pi\,\Delta\Phi_0^2 = 2\pi\frac{\Delta k_0}{|k_\mathrm{p}|} \cdot \tag{14}$$

On the other hand, it can be seen from Figure 2b that the divergence $\Delta\Phi_0$ around a non colinear phase matching configuration is given, if Φ_0 remains small, by the

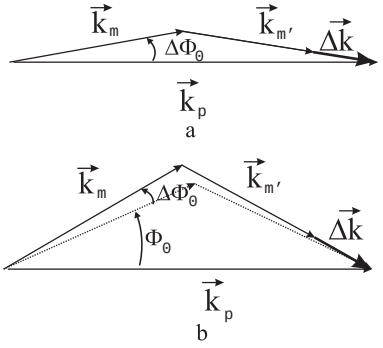

Fig. 2. Mismatch vectors for a colinear phase matching configuration (a) and for a non colinear phase matching configuration (b).

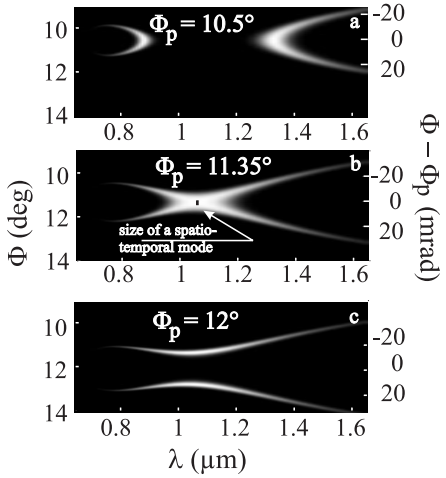

Fig. 3. Results showing in gray levels the amplification transfer function calculated around degeneracy for different angles Φ_p. The elementary cell representing a spatio-temporal fluorescent mode is shown in (b).

equation:

$$\Delta\Phi_0 = \frac{\Delta k_0}{|k_\mathrm{p}|\sin\Phi_0} \cdot \tag{15}$$

where Φ_0 is the angle between $\mathbf{k}_\mathrm{p}$ and $\mathbf{k}_m$ at perfect phase matching. The solid angle corresponding to the QPM ring is:

$$\Delta\Omega_0^\mathrm{nc} = 4\pi\,\sin\Phi_0\Delta\Phi_0 = 4\pi\frac{\Delta k_0}{|k_\mathrm{p}|} = 2\Delta\Omega_0^\mathrm{c}. \tag{16}$$

This solid angle remains constant whatever the small angle Φ_0 and is twice the solid angle obtained in the colinear configuration. By dividing the solid angles given by equations (14, 16) by the size of a spatial mode, we obtain $N_\mathrm{spatial}^\mathrm{c} \simeq 50$ and $N_\mathrm{spatial}^\mathrm{nc} \simeq 100$ in good accordance with the numerical results of Table 1.

Once the number of QPM spatial modes is determined, the evolution of the fluorescence power with wavelength around degeneracy can be calculated. Figures 3a to 3c show in gray levels a numeric calculation of the amplification transfer function $ATF_{\Theta=90°}(\Phi, \lambda)$ calculated

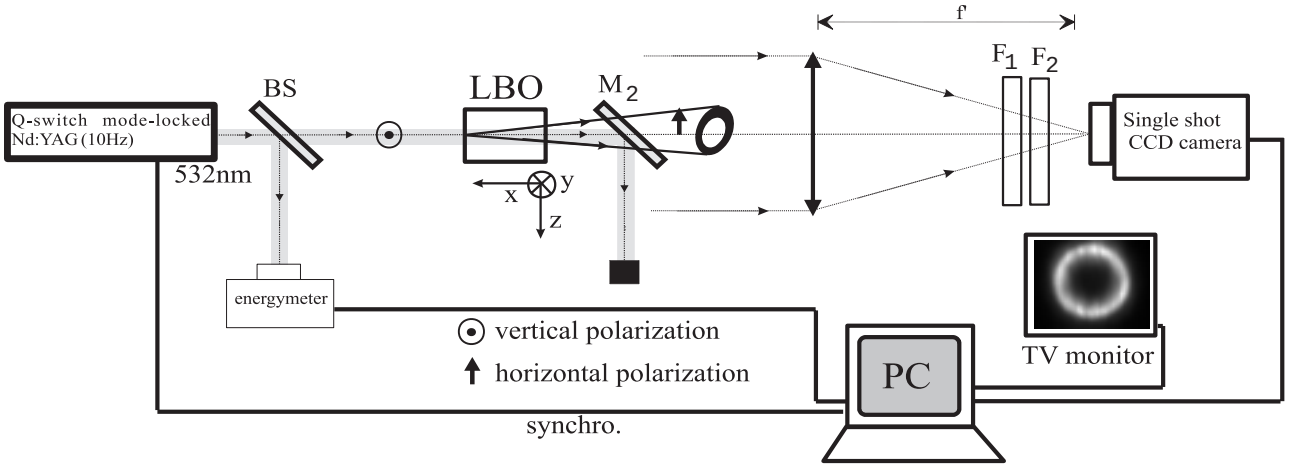

Fig. 4. Experimental set-up used to study the spatial properties of parametric fluorescence.

around degeneracy for different propagation directions of the pump plane wave in the (XY) LBO crystal plane ($\Theta_{\rm p} = 90°$). The mean parametric gain is equal to 10 cm^{-1}. Since no light is emitted at degeneracy for $\Phi_{\rm p} = 10.5°$ (Fig. 3a), parametric photons are generated around 900 nm and 1.3 μm in cones of 10 and 20 mrad bandwidth respectively, centered on the pump wave direction. When $\Phi_{\rm p}$ is equal to 11.35° (Fig. 3b) there is a maximum of QPM modes around degeneracy in a 10 mrad bandwidth cone and over a 200 nm wavelength range. This phase matching configuration was previously used for demonstrating the amplification of polychromatic images [16,17]. When $\Phi_{\rm p}$ is greater than 11.5° (Fig. 3c) parametric light is no longer generated in the pump wave direction, but rather in a ring around the pump wave direction over a 200 nm wide wavelength range. Since the size of a temporal mode depends on the characteristics of the pump pulse, we assume that it is equal to 100 GHz. The size of the corresponding elementary cell is indicated in the Figure 3b. The number of QPM modes $N_{\rm temporal}$ is obtained for a given phase matching condition by dividing the QPM frequency bandwidth by the size of a temporal mode.

$$N_{\rm temporal} = \frac{\text{QPM bandwidth}}{\text{temporal mode size}}\,. \qquad (17)$$

We observe from Figure 3 that the QPM bandwidth remains constant for different phase matching conditions and the number of QPM temporal modes is about 600. This value can be analytically found. Indeed, in a type I crystal at degeneracy, colinear phase matching is non critical with the signal wavelength [16,17]. With a mode m frequency $\omega_m = \omega_0 + {\rm d}\omega$, the phase mismatch can be expressed as:

$$\Delta k = \frac{\Delta\omega^2}{c}\left(2\frac{\partial n}{\partial\omega} + \omega\frac{\partial^2 n}{\partial\omega^2}\right)_{\omega=\omega_0}. \qquad (18)$$

where $\partial n/\partial\omega$ and $\partial^2 n/\partial\omega^2$ are respectively the first and the second derivatives of the refractive index at degeneracy. For a phase mismatch $\Delta k_0 \simeq 5$ cm^{-1} (with a parametric gain of 10 cm^{-1} it corresponds to the phase mismatch limit where efficiency remains greater than 44%) the QPM frequency bandwidth is given by:

$$2\Delta\nu_0 = \frac{\Delta\omega_0}{\pi} = \frac{1}{\pi}\left[\frac{c|\Delta k_0|}{(2\frac{\partial n}{\partial\omega} + \omega\frac{\partial^2 n}{\partial\omega^2})_{\omega=\omega_0}}\right]^{\frac{1}{2}}. \qquad (19)$$

By taking in account of the Sellmeier coefficients of the LBO crystal [18], the calculation gives at degeneracy a bandwidth of 6×10^{13} Hz corresponding to 600 QPM temporal modes.

The total number of spatio-temporal QPM modes, for a given phase matching condition, is then obtained by the product $N_{\rm spatial}N_{\rm temporal}$.

4 Experimental results

In this section, we first consider the spatial properties of the fluorescence signal and then compare experimental results to the numeric simulation giving the number of spatial QPM modes. Figure 4 shows the experimental set-up. Pump pulses are delivered by a frequency-doubled Q-switch mode-locked Nd:YAG laser. The pulses at 532 nm have an elliptical transverse section ($2\Delta x_{\rm pump} = 0.44$ mm, $2\Delta y_{\rm pump} = 0.12$ mm) and a 43 ps time duration. The time-bandwidth product is close to 1. The repetition rate is 10 Hz. The pump beam is vertically polarized in the (XY) plane of a 15 mm long LBO crystal whose lateral dimensions are 4×4 mm^2. A beam splitter (BS: $R = 10\%$, $T = 90\%$) in front of the crystal permits the measurement of the pump pulse energy with a energymeter. The transmitted part of the collimated pump beam illuminates the input face of the crystal and a dichroic mirror separates it from the fluorescence signal at the output of the crystal. The spatial frequency spectrum of the parametric fluorescence is imaged in the image focal plane of lens L_1 (Fourier plane) by a single-shot CCD camera. A RG5 filter (F_1) and a narrow band interference filter (F_2: $\Delta\lambda_{\rm IF} = 4.8$ nm, $\Delta\nu_{\rm IF} = 1.27$ THz @1064 nm) in front of the CCD camera limit the number of temporal detected modes around degeneracy. The CCD camera

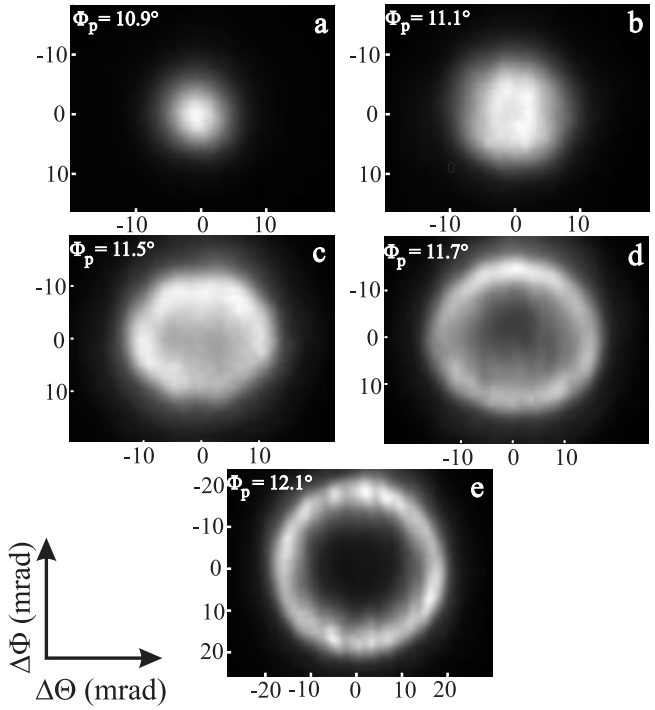

Fig. 5. Fluorescence energy (at degeneracy) with respect to the angle Φ_{p}. The mean pump energy is 0.5 mJ per pulse. Spatial inhomogeneities with sizes corresponding to one spatial mode can be observed in (c–e).

and the energymeter are monitored by a computer synchronized with the laser. Hence, the far field distribution of the fluorescence signal is measured shot by shot with respect to the pump pulse energy. Tuning the direction of propagation of the pump beam in the (XY) crystal plane is achieved by tilting the crystal around the Z axis.

Figures 5a–5e show experimental spatial frequency spectra of the parametric fluorescence for different propagation directions of the pump beam in the (XY) plane. The mean energy per pump pulse is 0.5 mJ. The vertical and horizontal axes are graduated in angle. For Φ_{p} lower than 10.9°, no parametric fluorescence is detected. For $10.9° < \Phi_{\mathrm{p}} < 11.3°$ fluorescence is generated in a cone around the pump beam direction (Figs. 5a and 5b) and then in a ring around the pump beam direction when Φ_{p} exceeds 11.3° (Figs. 5c–5e). The shapes of the spatial frequency spectra are in a good agreement with the calculated $ATF's(\Phi, \Theta)$ presented in Figure 1. In order to integrate the fluorescence power, we have assumed that the spectral sensitivity of the CCD camera remains constant over the narrow band of the interferential filter. Hence, the total number of gray levels in an image is proportional to the total energy emitted in this range. The CCD camera was previously calibrated at 1.064 μm in order to determine the coefficient of proportionality.

Figures 6a–6c represent the single-shot measurements of the energy of parametric fluorescence with respect to the energy of the pump pulses for three different propagation directions of the pump beam. The corresponding experimental spatial frequency spectra are shown in the

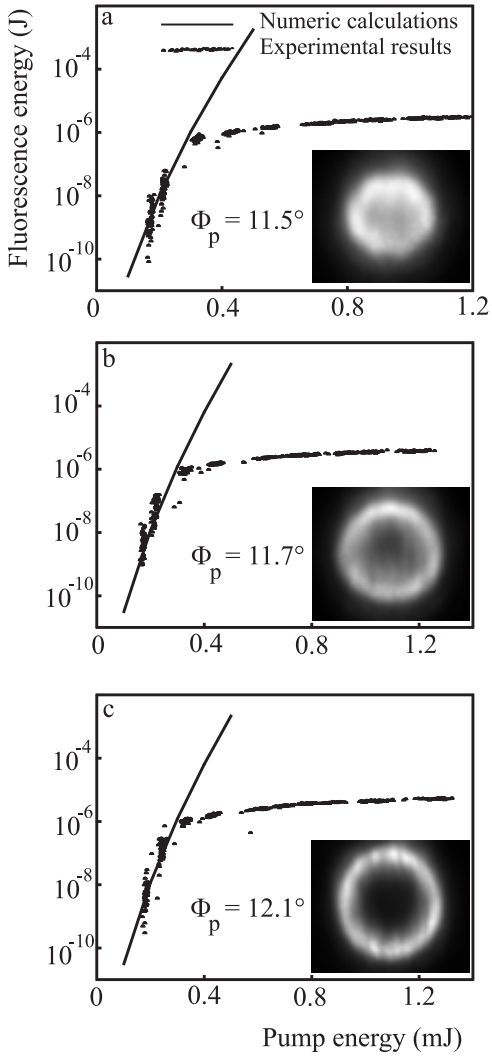

Fig. 6. Experimental single-shot measurements of the fluorescence signal energy with respect to the pump energy for three different phase-matching conditions. Solid curves show results from numeric calculations of the output fluorescence power in the undepleted pump approximation.

inserts. The fluorescence level grows exponentially until a pump energy of 0.4 mJ is attained. For greater energies, the fluorescence level saturates because of the pump beam depletion. These measurements have been compared with a numerical estimation of the global fluorescence power (solid curves in Fig. 6). To obtain a realistic estimation of this power, the field at the input face of the crystal has been considered as a superposition of plane waves, with a constant brightness (*i.e.* intensity by solid angle unit) whatever the propagation direction. This value has been determined in order to correspond to one photon per spatial mode. Hence, the total number of equivalent quantum noise photons at the input for one temporal modes is given by (see Eq. (1)):

$$N_{\mathrm{total}} = \frac{Sn^2}{\pi(0.31\lambda)^2} \cdot \tag{20}$$

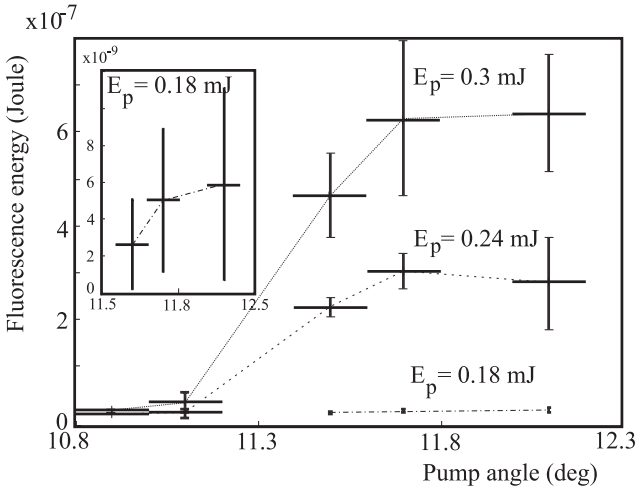

Fig. 7. Fluorescence energy (at degeneracy) with respect to the angle $\Phi_{\rm p}$ for different pump pulse energies. The points of this figure have been obtained by fitting with four order polynomials the experimental points of Figure 6. This fitting was necessary in order to obtain data at given pump energy levels, despite experimental fluctuations of the pump power.

For our crystal ($S = 0.16$ mm^2, $n = 1.60$, $\lambda = 1.064$ μm), it gives 1.2×10^8 photons. However, a very few of these modes are amplified because of phase matching and the narrow section of the pump beam. Once the input power has been determined, the total output power has been calculated simply by adding the output power calculated from equation (8) for each mode. In the undepleted pump range, the experimental results are in good accordance with the numeric calculations. The uncertainty on the measurement of the pump power leads to uncertainties in the corresponding expected fluorescence level and the low efficiency of the CCD camera at 1.064 μm did not allowed us to detect fluorescence levels lower than 0.1 nJ. Figure 7 represents the fluorescence level at degeneracy with respect to the propagation direction of the pump wave in the (XY) crystal plane for different energies of the pump beam in the undepleted range. The measurements correspond to spatial frequency spectra of Figures 5a–5e. The fluorescence level increases when the pump beam direction is tuned from 11° to 11.7° and can be considered as constant for $\Phi_{\rm p} > 11.7°$ as it was theoretically predicted in equation (16).

Our calculation used an equivalent input quantum noise on the entire crystal section and the power of the very narrow fluorescence beam has been determined classically in good agreement with the experiment. A question remains to answer. How many modes are efficiently amplified? The answer may be given in the following way. The number of amplified spatial modes can be defined as the total fluorescence energy for one temporal mode divided by the fluorescence energy due to one input photon for perfect phase matching and the maximum pump intensity. 5 spatial modes and 12 temporal modes, defined in a similar way, are obtained. However, it should be noted that, because of the exponential dependence between the fluorescence power and the pump amplitude, experimental uncertainties on the exact spatio-temporal repartition of the pump beam result in an uncertainty of one order of magnitude about the total number of amplified modes. An other way to count the number of amplified modes consists in associating the area of the fluorescence beam at the output of the crystal with its reciprocal area in the spectral (spatial frequencies) domain. After division by the wavelength in the crystal, this area is defined in units of solid angle and the number of amplified modes is obtained by dividing the QPM area by this area, like in equation (12). To determine the size of the fluorescence beam, we performed a numerical simulation of its propagation through the crystal. The result gives:

$$\begin{cases} 2\Delta x_{\rm fluo} = 63\ \mu{\rm m}, \\ 2\Delta y_{\rm fluo} = 38\ \mu{\rm m}. \end{cases} \tag{21}$$

Where $(2\Delta x_{\rm fluo}, 2\Delta y_{\rm fluo})$ are the widths of the beam, at 44% of the maximum. The associated angular sizes of the mode are:

$$\begin{cases} 2\Delta\theta_{\rm fluo} = 10\ {\rm mrad}, \\ 2\Delta\phi_{\rm fluo} = 17\ {\rm mrad}. \end{cases} \tag{22}$$

Because of the small section of the fluorescence beam in the near field, these dimensions are greater than that of the ATF's ring and use of equation (12) to count the modes seems questionable. However, it is clear from the preceding paragraphs that the total power and the section of the fluorescence signal are, for a given pump intensity, proportional to the section of the pump beam. Hence, using equation (12) gives a correct estimation of the number of modes even if fractions of modes are involved. The result is, for a ring configuration, 1.2 spatial mode. This analysis is valid except for very narrow pump beams, where more complex phenomena are involved like natural trapping of beams [28] (low pass phase matching configuration) or generation of vortices [29] (band pass configuration).

The temporal properties of the parametric fluorescence were then studied with the experimental scheme of Figure 8. At the output of the crystal, the fluorescence signal illuminates the vertical input slit of a grating spectrometer (transmission grating G with 157.5 lines/mm). The temporal spectrum is detected by the single-shot CCD camera. Figures 9a–9e show experimental spectra for different propagation directions of the pump beam in the (XY) crystal plane. The mean pump energy is 1.3 mJ. The vertical axis corresponds to the spatial frequency associated to the angle Φ. As the quantum efficiency of the silicium CCD detector is very low in the $1-1.5$ μm range, only the short wavelength side of the fluorescence spectra is detected (range $0.75-1.1$ μm). Nevertheless the detected temporal spectra are in a good agreement with the numeric simulations of Figure 3. For colinear phase matching ($\Phi_{\rm p} \simeq 11.3°$, Fig. 9d) light is emitted around the pump wave direction in a 10 mrad spatial bandwidth cone and over a 200 nm spectral bandwidth. Like spatial

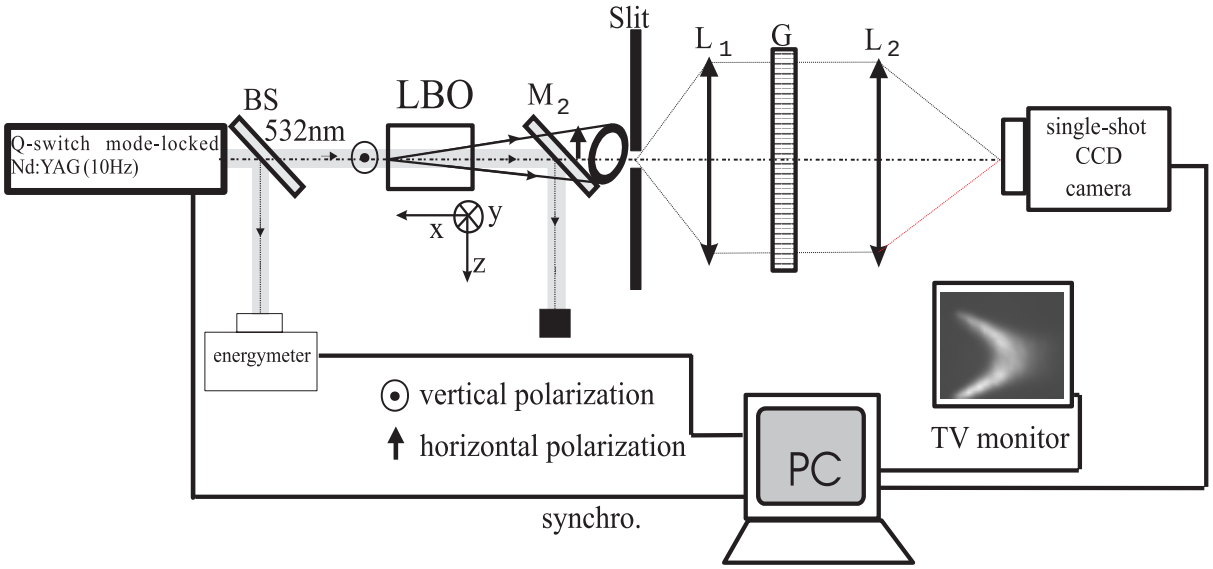

Fig. 8. Experimental set-up used to study the temporal properties of parametric fluorescence around degeneracy.

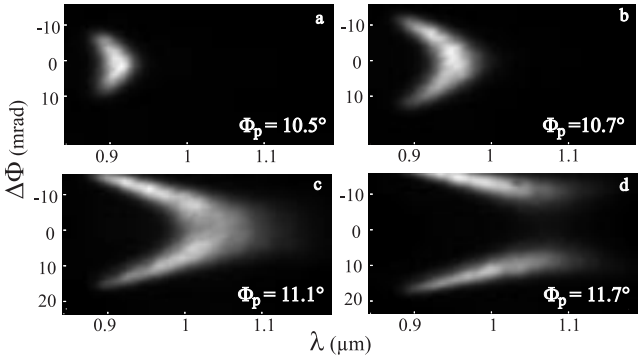

Fig. 9. Experimental temporal spectra of the parametric fluorescence emitted around degeneracy for different angles Φ_p. The pump energy is about 1.3 mJ per pulse. The vertical axis corresponds to the spatial frequency associated to the angle Φ.

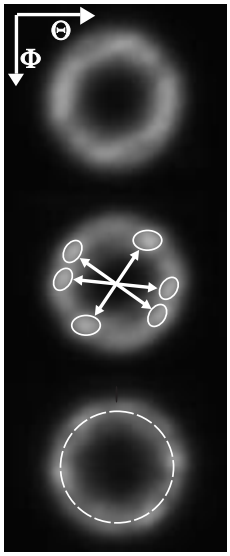

Fig. 10. A sequence of spatial frequency spectra obtained with the same phase matching condition and approximately the same pump energy. Each spectrum corresponds to one laser shot. Arrows on the second spectrum underline the central symmetry of the inhomogeneities. The circle of best phase matching, corresponding to the pixels used in Figure 11, is drawn on the third spectrum.

frequency spectra, the temporal spectra are similar to the temporal ATF's obtained in our previous works on parametric amplification of polychromatic images [16,19].

5 Fluctuations of fluorescence: spatial correlation and contrast

Intensity inhomogeneities can be observed in the rings of Figure 5. Figure 10 represents a sequence of three spatial frequency spectra obtained for the same phase matching conditions ($\Phi_p \simeq 11.9°$) and with approximately the same pump pulse energy. The spatial distribution of the inhomogeneities fluctuates from one shot to another. However, spatial correlation between pairs of spatial modes that are symmetrically distributed around the pump beam direction is clearly exhibited. Figure 11 shows the experimental autocorrelation functions along a circular profile corresponding to best phase matching [20]. The most prominent feature of these functions is the almost

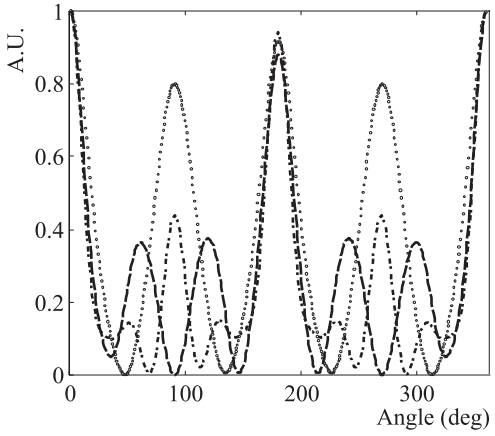

Fig. 11. Autocorrelation functions of the 1D intensity profiles obtained on the best phase matching circles of the three spectra of Figure 10. The continuous background has been removed.

perfect correlation for a angle of 180°. It means that fluctuations of areas that are opposite to each other with respect to the pump direction are strongly correlated. This effect, due to the emission of twin photons, has been extensively studied in the time domain [21]. In the spatial domain, numerous effects due to quantum correlations have been investigated by the group of Lugiato [22], especially in cavities [23]. Some aspects of quantum correlations in traveling wave amplification are also theoretically discussed in papers of Kolobov *et al.* [24,25]. Experimentally, twin beams corresponding to the parametric amplification of an image point [26] or of a spatial frequency [27] have shown strong temporal correlations. To our knowledge, this paper presents the first experimental characterization of the autocorrelation function of purely spatial fluctuations [30]. The quantitative connection between this result and the theoretical quantum correlation function of a traveling wave amplifier is beyond the scope of this paper. However it can bee seen in Figure 11 that the number of independent peaks of the autocorrelation function roughly corresponds to the number of amplified spatial modes.

6 Conclusion

We have presented a theoretical and experimental study of the spatio-temporal properties of the parametric fluorescence around degeneracy in a type I LBO crystal. The correspondence between a spatial mode and a resolution cell defined in our previous works on parametric image amplification has been demonstrated and extended to the spatio-temporal case. By numbering the quasi-phase matched detected spatio-temporal modes, the mean number of generated photons has been predicted. Spatial correlation between intensity fluctuations of the signal-idler pairs of modes has also been experimentally demonstrated.

References

1. W. Louisell, A. Yariv, A. Siegman, Phys. Rev. **124**, 1646 (1961).
2. D. Magde, H. Mahr, Phys. Rev. Lett. **18**, 905 (1967).
3. S. Haris, M. Oshman, R. Byer, Phys. Rev. Lett. **18**, 732 (1967).
4. J. Pearson, A. Yariv, U. Ganiel, Appl. Opt. **12**, 1165 (1973).
5. R. Byer, S. Haris, Phys. Rev. **168**, 1064 (1968).
6. K. Haldi, M. Sundheimer, P. Aschieri, P. Baldi, M. De Micheli, D. Ostrowsky, F. Laurell, J. Opt. Soc. Am. B **14**, 3197 (1997).
7. A. Yariv, *Quantum Electronics*, 3rd edn. (John Wiley and Sons, New York, 1989), pp. 430-435.
8. E. Cheung, K. Koch, G. Moore, J. Liu, Opt. Lett. **19**, 168 (1994).
9. K. Koch, E. Cheung, G. Moore, S. Chakmakjian, J. Liu, IEEE J. Quant. Electron. **31**, 769 (1995).
10. F. Devaux, E. Lantz, A. Lacourt, D. Gindre, H. Maillotte, P. Doreau, T. Laurent, Nonlin. Opt. **11**, 25 (1995).
11. S. Prasad, J. Opt. Soc. Am. A **11**, 2799 (1994).
12. A. Gatti, L.A. Lugiato, G. Oppo, R. Martin, P. Di Trapani, A. Berzanskis, Opt. Expr. **1**, 21 (1997).
13. F. Devaux, E. Lantz, Opt. Commun. **114**, 295 (1995).
14. In the case of Gaussian beams, this value corresponds to bandwidths (Δt, $\Delta \nu$) giving a product $\Delta t \Delta \nu = 1$.
15. K. Bencheikh, E. Huntziger, J. Levenson, J. Opt. Soc. Am. B **12**, 847 (1995).
16. F. Devaux, E. Lantz, J. Opt. Soc. Am. B **12**, 2245 (1995).
17. E. Lantz, L. Han, A. Lacourt, J. Zyss, Opt. Commun. **97**, 245 (1993).
18. C. Chen, Y. Yu, A. Jiang, B. Wu, G. You, R. Liand, S. Lin, J. Opt. Soc. Am. B **6**, 616 (1989).
19. F. Devaux, Ph.D. thesis, UFR des Sciences et Techniques de l'Université de Franche-Comté, 1996.
20. The center of these circular profiles has been precisely determined thanks to the almost perfect axial symmetry of the fluctuations, using an algorithm originally designed for determining the axis of turbofan engines that present the same symmetry: L. Oriat, E. Lantz, Patt. Recogn. **31**, 761 (1998).
21. See for example: A. Heidmann, R. Horowicz, S. Reynaud, E. Giacobino, C. Fabre, G. Camy, Phys. Rev. Lett. **59**, 2555 (1987).
22. For a review, see: L. Lugiato, M. Brambilla, A. Gatti, Adv. At. Mol. Opt. Phys. **40**, 229 (1998).
23. I. Marzoli, A. Gatti, L. Lugiato, Phys. Rev. Lett. **78**, 2092 (1997).
24. M. Kolobov, I. Sokolov, Sov. Phys. JETP **69**, 1097 (1989).
25. M. Kolobov, I. Sokolov, Europhys. Lett. **15**, 271 (1991).
26. T. Pittman, Y. Shih, D.V. Strekalov, A. Sergienko, Phys. Rev. A **52**, 3429 (1995).
27. M.L. Marable, S. Choi, P. Kumar, Opt. Expr. **2**, 84 (1998).
28. P. Di Trapani, A. Berzanskis, S. Minardi, S. Sapone, W. Chinaglia, Phys. Rev. Lett. **80**, 265 (1998).
29. P. Di Trapani, A. Berzanskis, S. Minardi, S. Sapone, W. Chinaglia, Phys. Rev. Lett. **81**, 5133 (1998).
30. Some related results are given in B.M. Jost, A.V. Sergienko, A.F. Abarraddy, B.E.A. Salek, M.C. Teich, Opt. Expr. **3**, 81 (1998).